

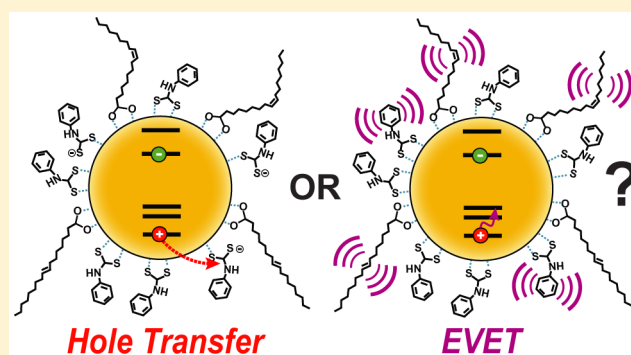
Can Exciton-Delocalizing Ligands Facilitate Hot Hole Transfer from Semiconductor Nanocrystals?

Michael S. Azzaro,[†] Mark C. Babin,[†] Shannon K. Stauffer,^{†,‡} Graeme Henkelman,^{†,‡} and Sean T. Roberts^{*,†}

[†]Department of Chemistry and [‡]Institute for Computational Engineering and Sciences, The University of Texas at Austin, Austin, Texas 78712-1224, United States

Supporting Information

ABSTRACT: Exciton-delocalizing ligands (EDLs) are of interest to researchers due to their ability to allow charge carriers to spread into the ligand shell of semiconductor nanocrystals (NCs). By increasing charge carrier surface accessibility, EDLs may facilitate the extraction of highly photoexcited carriers from NCs prior to their relaxation to the band edge, a process that can boost the performance of NC-based photocatalysts and light harvesting systems. However, hot carrier extraction must compete with carrier cooling, which could be accelerated by the stronger interaction of charge carriers and EDLs. This report describes the influence of the EDL phenyldithiocarbamate (PTC) on the electron and hole cooling rates of CdSe NCs. Using state-resolved transient absorption spectroscopy, we find that PTC treatment accelerates hole cooling by a factor of 1.7. However, upon further treatment of these NCs with cadmium(II) acetate, the hole cooling rate reverts to the value measured prior to PTC treatment, yet these NCs maintain a red-shifted absorption spectrum indicative of PTC bound to the NC surface. This result provides strong evidence for the existence of two distinct surface-bound PTC species: one that traps holes before they cool and can be removed by cadmium(II) acetate, and a second species that facilitates exciton delocalization. This conclusion is supported by both DFT calculations and photoluminescence measurements. The outlook from our work is that EDLs do not necessarily lead to an acceleration of carrier cooling, suggesting that they may provide a path for hot carrier extraction.



I. INTRODUCTION

Semiconductor nanocrystals (NCs) have been of great interest to researchers as novel optoelectronic materials due to their tunable bandgaps, high molar extinction, and solution processability. However, their integration into commercial electronics remains challenging due to modest electron and hole mobilities ($\sim 10^{-4}$ cm²/(V s)) in NC thin films.¹ During colloidal synthesis, long aliphatic “native ligands” (NLs) are introduced to the reaction to terminate particle growth and impart solubility to the NCs. However, when cast into a solid film, NLs physically separate NCs, creating a large potential energy barrier for charge transfer between them that limits carrier mobility. For applications such as photocatalysis^{2–4} and solar energy harvesting,^{5–8} where charge carriers must be extracted from NC films, NLs are problematic and hinder device performance.

To circumvent this issue, researchers have developed methods to postsynthetically modify NC surfaces by exchanging insulating NLs for ones that improve carrier mobility.^{8–12} One method is to use ligands that are electrically conductive as a type of “molecular solder” to wire NCs together in a close-packed film.¹⁰ This method is particularly attractive due to its ability to control inter-NC spacing through the size of the

ligand and allow carrier wave functions to spread into the ligand shell through stronger NC–ligand electronic coupling, a process termed “exciton delocalization”.¹³ By using exciton-delocalizing ligands (EDLs) to extend charge carrier density beyond the NC core and into the ligand shell, wave function overlap between neighboring NCs can be improved, increasing carrier mobility by orders of magnitude in some cases.¹⁰ Indeed, following the exchange of NLs for Na₂Cd₂Se₃ ligands, Talapin and co-workers have measured electron mobilities of nearly 450 cm²/(V s) in CdSe NC field effect transistors (FETs),¹⁰ a value comparable to that of single crystal and polycrystalline silicon FETs (100–1000 cm²/(V s)).^{14,15} Zotti and co-workers have also demonstrated proof of this concept using exciton-delocalizing bis(dithiocarbamate)-based ligands, which improved photocurrent generation by 2 orders of magnitude in NC films compared to their carboxylate-based structural analogues.¹¹

While reports examining the impact of EDLs on mobility and device efficiency have appeared, only recently have studies

Received: August 12, 2016

Revised: October 22, 2016

Published: November 21, 2016

emerged that examine the kinetics of charge carrier transfer facilitated by these ligands.^{16–18} A recent report has demonstrated subpicosecond transfer of photoexcited holes in CdS NCs to a molecular acceptor linked to the NC surface by the EDL phenyldithiocarbamate (PTC).¹⁹ The rapid time scale observed for this transfer suggests that it may be fast enough to compete with hole cooling. If EDLs can facilitate hot carrier transfer, this would be an exciting development as it would provide unique opportunities for advancing both photocatalysis²⁰ and solar energy applications²¹ where harvesting charges with excess energy could both improve the efficiency of these processes and provide access to previously inaccessible photodriven reactions. While hot electron cooling in NCs occurs through Auger energy transfer to holes,²² no such relaxation channel exists for excited holes due to the larger energy level spacing in the conduction band (CB) with respect to the valence band (VB).^{23,24} Therefore, it is expected that hole cooling primarily occurs through electronic to vibrational energy transfer (EVET) pathways, some of which involve direct vibrational energy transfer to surface bound ligands.^{25,26} Thus, one potential cause for concern is that the strong association between charge carriers and EDLs that extends carrier wave functions into the ligand shell may also facilitate rapid carrier cooling via EVET, hindering the prospects of using EDLs to harvest hot carriers. However, a study by Schnitzenbaumer and co-workers¹⁸ found that while carrier cooling rates are impacted by surface-bound EDLs, the origin of these changes is not obvious.

Previously, to determine the impact of ligands on carrier cooling, three-pulse experiments were carried out in which the decay of hot carriers was directly monitored with mid-IR pulses following above bandgap excitation.²⁷ These pump–repump–probe experiments have measured carrier cooling in CdSe NCs by directly pumping and probing intraband transitions as a function of surface ligand identity. While this experiment directly measures intraband cooling, the difficulty of generating short mid-IR pulses, lack of efficient detectors in this spectral region, and three pulse nature of this experiment have limited its usage in studying NC carrier cooling. To alleviate these issues, Kambhampati and co-workers developed a method of measuring NC carrier cooling dynamics using two-pulse transient absorption experiments.²⁸ By preparing different initial excitonic states and watching how spectral features evolve at early times, differences between measured kinetic traces can be used to extract time scales that reflect the intrinsic carrier cooling rates of a system. With this technique, denoted state-resolved transient absorption (SR-TA), we can address questions regarding how surface coverage impacts NC cooling dynamics.

The EDL described above, PTC, has been studied extensively by Weiss and co-workers^{13,29–31} because of its large impact on metal–chalcogenide NC absorption. When bound to CdS NCs, PTC can lower the bandgap of these materials by nearly 1 eV through mixing of its HOMO with occupied states near the NC band edge, forming hybrid states wherein holes partially reside in the PTC ligand shell.^{13,32} This has led us to choose this particular EDL as our system for study in this report. We have used SR-TA^{18,28,33,34} to determine the effect of the EDL, PTC, on cooling dynamics in 2.8 nm diameter CdSe NCs. To do so, we have investigated three samples: CdSe NCs capped with oleic acid (CdSe-OA), CdSe NCs initially capped with oleic acid that has been partially ligand exchanged for PTC (CdSe-PTC), and CdSe-PTC samples treated with cadmium(II)

acetate (PTC + Cd(Ac)₂) to remove unbound PTC as prior reports³¹ have suggested diffusive quenching of CdSe-PTC by free PTC molecules in solution. Using SR-TA, we find an apparent increase in the hole cooling rate of CdSe-PTC by nearly a factor of 2 relative to CdSe-OA. This effect is reversed upon treatment of NCs with Cd(Ac)₂, yet these NCs maintain a red-shifted absorption spectrum indicating that PTC remains bound to the NC surface. Thus, rather than ascribing the enhancement of the hole cooling rate to EVET, we assign it to fast ligand-associated trapping by PTC molecules bound to NC surfaces in CdSe-PTC. This fast trapping pathway is then eliminated via modification of these PTC trap sites by Cd(Ac)₂. Evidence for this picture is supported by DFT calculations as well as FT-IR and steady-state and time-resolved photoluminescence measurements. This data suggests that hot carrier extraction may be feasible in PTC-capped NCs, as we see fast trapping pathways in CdSe-PTC that are competitive with hole cooling to the band edge.

II. EXPERIMENTAL AND THEORETICAL METHODS

Synthesis of CdSe Nanocrystals. CdSe NCs were synthesized using a modified literature method³⁵ in which cadmium(myristate)₂ (170 mg), powdered selenium (12 mg), and 90% technical grade 1-octadecene (18 mL) were added to a three-neck round-bottom flask, vacuumed for 1 h, and heated to 240 °C under N₂ flow while being stirred vigorously. The solution was heated at 240 °C until it reached a color indicative of NCs of a desired size, at which point 1 mL of 90% technical grade oleic acid was injected to the solution. The solution was then allowed to stir for ~3 min at 240 °C before cooling to room temperature. To remove the solvent, the resulting mixture was dispersed in ethanol and centrifuged at 3200 rpm for 10 min. The supernatant was removed, and this process repeated until a dry pellet was formed. This solution was dispersed in a 1:1 (v/v) mixture of hexane and ethanol and centrifuged for 10 min at 3200 rpm to remove excess capping agent and cadmium precursor. The liquid phase was removed, and this process was repeated in triplicate before allowing the films deposited on centrifuge tubes to air-dry overnight. NCs were then dispersed in dichloromethane (DCM) for spectroscopic characterization.

Synthesis of Phenyldithiocarbamate. Phenyldithiocarbamate (PTC) was synthesized via a modified literature procedure³⁶ by chilling 5 mL of aniline in 30 mL of 30% w/w sodium hydroxide to 0 °C while stirring vigorously under N₂ flow. To this solution, 5 mL of carbon disulfide was added dropwise over 15 min, and the solution was allowed to stir for 45 min before returning to room temperature. The resulting yellow precipitate was subsequently isolated via vacuum filtration, washed with dichloromethane, and stored in a desiccator in the dark. The final product was a fine white powder.

PTC Ligand Exchange. Solution exchanges were performed in DCM. 125–5000 mol equiv of PTC was added to a solution of ~10 μM NCs that was then stirred in the dark for 4–24 h depending on the sample. Following the exchange, the solution was passed through a 0.45 μm syringe filter to remove any undissolved PTC or aggregated NCs from solution.

Cd(Ac)₂ Addition. Addition of Cd(Ac)₂ was performed by adding 50 μL of methanol and 1000 mol equiv of Cd(Ac)₂ to a solution of ~10 μM NCs in DCM. The resulting solution was then sonicated in the dark for 2 h. Following sonication, the

solution was passed through a 0.45 μm syringe filter to remove any undissolved $\text{Cd}(\text{Ac})_2$ or aggregated NCs.

Steady-State Absorption Spectroscopy. Samples were prepared by dissolving purified NC pellets in DCM, and absorption spectra were collected on a Shimadzu UV-2600 spectrometer using a 1 mm path length near-IR transmissive quartz cuvette. Prior to collecting each spectrum, a DCM blank was obtained in the same cuvette for each sample such that the spectra were baseline corrected from sample to sample. FT-IR measurements were carried out on a Bruker Vertex 70 infrared spectrophotometer over a spectral window of 500–4000 cm^{-1} with a resolution of 0.5 cm^{-1} . FT-IR samples were prepared by drop-casting 60 μL of a 50 mg/mL solution of CdSe-OA in 1:1 (v/v) hexane:octane on 1 mm thick CaF_2 substrates. After recording both UV–vis and FT-IR absorption spectra of the CdSe-OA film, the sample was soaked in a solution of 10 mM PTC in methanol for 4 h. After collecting spectra of the ligand-exchanged CdSe-PTC film, the sample was further treated by soaking it in a 5 mM $\text{Cd}(\text{Ac})_2$ solution in methanol for 2 h, with spectra collected every 30 min. The baseline for each recorded spectrum was corrected by fitting the data in nonabsorbing regions to a cubic spline function.

Steady-State Photoluminescence. Solutions for photoluminescence were diluted in DCM to an optical density below 0.05 in a 1 cm quartz cuvette at the excitation wavelength of $\lambda_{\text{Ex}} = 402$ nm. Emission spectra were collected on a Horiba Jobin Yvon Fluorolog3 spectrofluorometer in a front face collection geometry. Emission and excitation slit widths were set to 5 nm resolution.

Time-Resolved Photoluminescence. Time-correlated single photon counting (TCSPC) was performed using a Horiba Jobin Yvon Fluorolog3. NC suspensions were placed in a 1 cm path length quartz cuvette excited using a nanoLED with a peak emission wavelength of 402 nm. Emission from sample solutions was collected at a right angle relative to the path of the excitation source using a slit width commensurate with a 2 nm spectral window. To prevent the reabsorption of photons emitted by each sample, NC solutions were diluted such that they had an optical density below 0.05 at the excitation wavelength of 402 nm. Emission traces were collected over a 200 ns window, resulting a bin width of 0.0549 ns/collection channel. Spectra were collected at their respective emission peaks, which ranged from 535 to 555 nm. The instrument response associated with each sample trace was collected using an ideal scattering solution and typically had a fwhm of 670 ps.

Transient Absorption. A femtosecond Ti:sapphire regenerative amplifier (Coherent Legend Duo Elite, 3 kHz, 4.5 mJ) was used to generate ~ 90 fs pulses centered at 804 nm with a bandwidth of 160 cm^{-1} (fwhm). A small portion of the amplifier output (~ 1 μJ) was focused into a 1 cm path length flow cell filled with distilled H_2O to produce broadband probe pulses (390–780 nm) via self-phase modulation. Tunable pump pulses (470–540 nm) were generated using a home-built noncollinear optical parametric amplifier (NOPA). Broadband pulses produced by the NOPA were temporally compressed and spectrally narrowed to 10 nm bandwidth (fwhm) using a Fastlite Dazzler AOM Pulse Shaper. Pump pulse fluence was adjusted such that all samples maintained an excitation density of less than 0.01 excitations per NC. All samples were diluted in a 1 mm path length cuvette and stirred vigorously throughout data collection. Wavelength-dependent instrument response functions (IRFs) for each scan were obtained using a 1 mm

path length cuvette filled with DCM. Collection of frequency-dependent IRFs allowed for chirp correction of the supercontinuum probe pulse. The temporal cross-correlation of the pump and probe was found to be ~ 95 fs (fwhm) averaged across the probe spectrum. For full details of the transient absorption spectrometer, chirp correction, and data analysis see the Supporting Information.

III. RESULTS AND DISCUSSION

PTC Ligand Exchange. CdSe NCs were synthesized using a modified literature method as described in the Experimental Methods section and were found to have a diameter of 2.8 nm based on sizing curves from Yu et al.³⁷ Figure 1A depicts

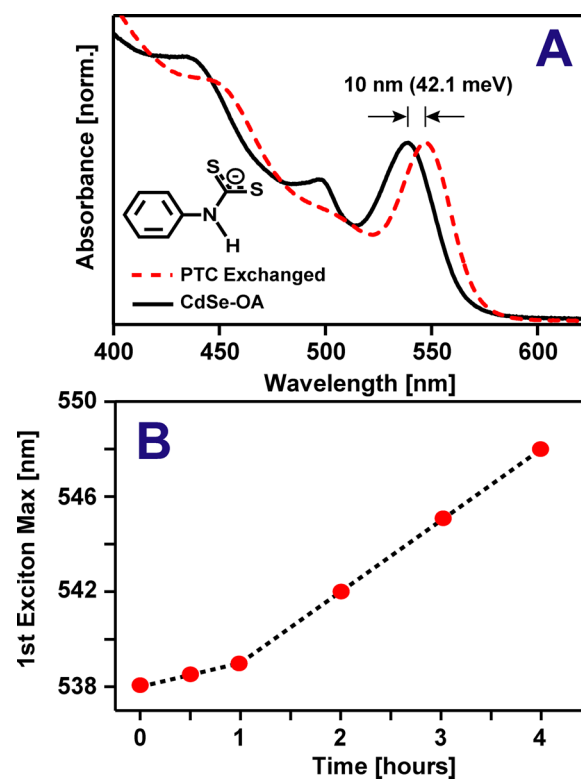


Figure 1. (A) Steady-state absorption spectra of 2.8 nm diameter CdSe NCs before (black) and after (dashed red) 4 h PTC exchange. (B) Kinetics showing the position of the first exciton peak maximum as a function of exchange time.

representative steady-state absorption spectra for CdSe NCs dispersed in DCM used for the time-resolved measurements in this study, while Figure 1B plots the position of the first excitonic peak as a function of exchange time. As previous reports have shown,^{13,29,30} the addition of PTC to a solution of CdSe NCs results in a red-shift of the absorption spectrum that has been attributed to exciton delocalization induced by the PTC ligand. The formation of new hybrid states between the NC orbitals and ligand frontier orbitals is hypothesized to lower the NC bandgap by providing the VB hole access to lower energy excitonic states. We have achieved bathochromic shifts of up to 75 meV for NCs of this size by allowing the exchange to proceed for >48 h. However, to complete the SR-TA experiments described below in a timely manner, we chose to terminate the exchange after 4 h, as during this time window the majority ($\sim 60\%$) of the total shift occurs. For spectra and

kinetics of the full 60 h exchange, see Figure S1 of the Supporting Information.

Assignment of Features in Transient Absorption Spectra. The top portion of Figure 2 shows a representative

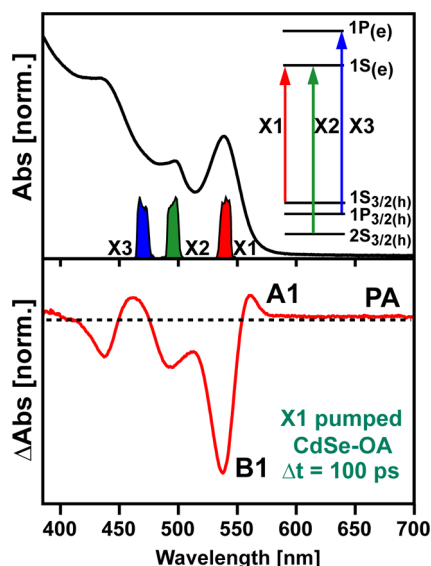


Figure 2. (top) Pump pulse spectra used for X1 (red), X2 (green), and X3 (blue) excitation overlaid on the absorption spectrum of CdSe-OA. (inset) Energy level diagram of CdSe NCs that highlights the X1, X2, and X3 excitonic states prepared by each pump pulse. (bottom) Transient absorption spectrum of CdSe-OA measured for a pump-probe time delay of 100 ps following X1 excitation. Important spectral features include B1 = population of the 1S_(e) electronic state, A1 = absorption of an X1 exciton in the presence of hot carriers, and PA = trapped holes.

absorption spectrum of CdSe-OA. Inset in this figure is a diagram of the electronic structure of CdSe NCs that assigns the three lowest energy peaks in the measured spectrum to transitions that excite the three lowest optically accessible excitonic states of the NC.³⁸ These excitonic states are labeled X1, X2, and X3, and the transitions that generate them are represented by red, green, and blue arrows from low to high energy. These “molecular-like”, discrete excitonic states arise from quantum confinement of the electron and hole wave functions by the physical dimensions of the NC, which causes their energy level spacing to spread out near the band edge.³⁸ This leads to the appearance of discrete absorbance peaks that are superimposed on a bulk semiconductor-like absorption spectrum.

Using SR-TA, we are able to extract rates for both hot electron cooling between the lowest energy states that comprise the CB edge, 1P_(e) and 1S_(e), and hot hole cooling from the excited 2S_{3/2}(h) to the 1S_{3/2}(h) state at the VB edge. In SR-TA, a femtosecond excitation pulse is used to excite a specific excitonic state, and its ensuing dynamics are read out by measuring spectral changes in the transmission of a white light supercontinuum probe pulse. In principle, this is no different than conventional transient absorption spectroscopy. However, information tied to hot carrier cooling can be isolated by comparing two measurements wherein different initial excitonic states are prepared.^{18,28} Rates for charge carrier recombination and hole trapping can also be extracted from this data and will be discussed below.

Plotted below the absorption spectrum in Figure 2 are excitation pulse spectra used for SR-TA measurements. The tunability of our excitation laser allows us to selectively excite either X1, X2, or X3. Following excitation of any of these excitonic bands, changes occur in the absorption spectrum of the NC sample that are highlighted by the transient absorption difference spectrum plotted in the lower portion of Figure 2. The relevant spectral features for extracting the rates described above are assigned as follows. The feature labeled B1 (~540 nm) is attributed^{22,39} to the ground state bleach of the band edge (X1) excitonic state. Because of the 8-fold degeneracy of the 1S_{3/2}(h) band edge hole state, the amplitude of the B1 feature reports directly on the population of the 1S_(e) electron state. The feature denoted A1 (~570 nm), commonly referred to as the “biexciton feature”, arises due to a shift in the band edge transition energy due to charge screening by a hot exciton.^{22,40} The weak, broad, induced absorption to the red of the A1 feature (~575–700 nm) labeled PA^{34,41,42} has been assigned to trapped holes in CdSe NCs by many authors following observation of an increased decay rate of this feature upon addition of hole accepting molecules to NC suspensions.^{18,42}

Figure 3 schematically depicts the use of SR-TA to measure both electron (top panel) and hole (bottom panel) cooling

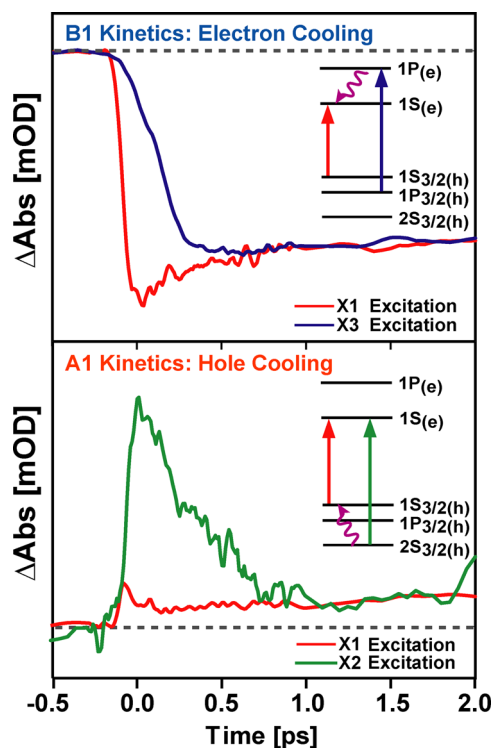


Figure 3. (top) X1 (red) and X3 (blue) pumped B1 kinetics of CdSe-OA. (inset) Energy level diagram of CdSe NCs depicting how electron cooling is isolated using X1 and X3 excitation. (bottom) X1 (red) and X2 (green) pumped A1 kinetics of CdSe-OA. (inset) Energy level diagram that highlights how hole cooling is isolated using X1 and X2 excitation.

processes. In the case of electron cooling, the transient kinetics of the B1 feature are compared following photoexcitation of the X1 and X3 excitons (see Figure 2). As the B1 feature is sensitive to the population of the 1S_(e) state, and not the cooling of the hole from 1P_{3/2}(h) → 1S_{3/2}(h), the only difference in the kinetic

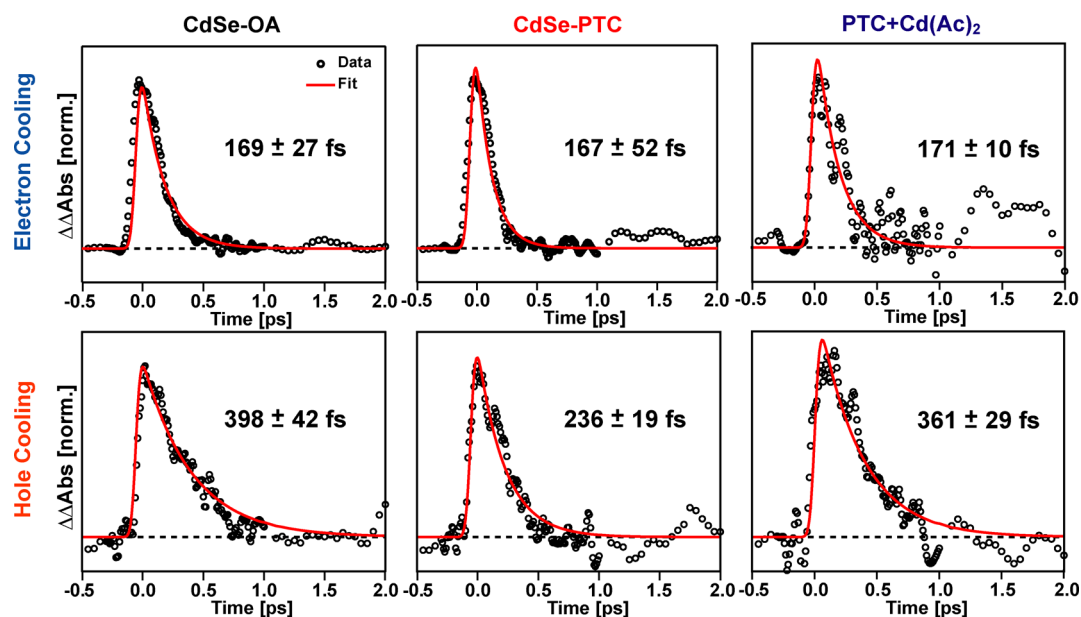


Figure 4. (top) Representative $\Delta\Delta A$ traces obtained for $1P_{(e)} \rightarrow 1S_{(e)}$ electron cooling rates. (bottom) Representative $\Delta\Delta A$ traces obtained for $2S_{3/2(h)} \rightarrow 1S_{3/2(h)}$ hole cooling rates. (inset) Average cooling time scales for multiple data sets with standard deviation.

traces for each of these excitations should be due to electron cooling from $1P_{(e)} \rightarrow 1S_{(e)}$. By taking the difference of kinetic traces for the B1 feature following X1 and X3 excitation, we can extract a time scale for $1P_{(e)} \rightarrow 1S_{(e)}$ cooling.

Similarly, hole cooling kinetics from $2S_{3/2(h)} \rightarrow 1S_{3/2(h)}$ can be obtained by detecting changes in the A1 induced absorption following X1 and X2 excitation (Figure 3, bottom). Since the A1 band arises from the Coulombic interaction between charge carriers and is dependent on their spatial separation, the difference of the A1 kinetics for these two pump frequencies should reflect the decay of the $2S_{3/2(h)}$ hole to the band edge. For both the B1 and A1 features, decay following the initial cooling of hot carriers should be identical after very short time delays (<2 ps). Therefore, the spectra were normalized between 3 and 4 ps to isolate carrier cooling dynamics at short time delays. In the following section we discuss the results of using this approach to determine variations in electron and hole cooling rates as a function of surface treatment.

Measuring Electron and Hole Cooling Rates with SR-TA. Using SR-TA, we measured the dependence of carrier cooling rates on surface treatment with the EDL PTC as well as treatment of the CdSe-PTC system with $\text{Cd}(\text{Ac})_2$ to remove unbound PTC molecules in solution.³¹ Following procedures employed by others for SR-TA experiments,^{18,28,33,34} Figure 4 shows the $\Delta\Delta A$ traces obtained from taking the difference of the corresponding kinetic traces for each sample: CdSe-OA, CdSe-PTC, and PTC + $\text{Cd}(\text{Ac})_2$. Fitting these $\Delta\Delta A$ traces allows us to extract the carrier cooling time scale for each sample.

Examining the $1P_{(e)} \rightarrow 1S_{(e)}$ electron cooling rates for each of our three samples (Figure 4, top row), we find that across the series the cooling rate is largely independent of the surface treatment. Electron cooling time scales for our measured samples are on the order of 170 fs, in good agreement with previously reported values for CdSe NCs of this size,¹⁸ and are likely due to Auger energy transfer to the photogenerated hole.^{22,25,43} This result indicates that PTC has little effect on electronic conduction band states, as is expected based on previous reports that PTC's LUMO energy is too high to mix

with CdSe CB states.³⁰ Additionally, this result indicates that electron and hole wave functions maintain spatial overlap, at least at short time delays, due to efficient Auger energy transfer to the VB hole.

Figure 4 (bottom) plots $2S_{3/2(h)} \rightarrow 1S_{3/2(h)}$ hole cooling rates for the same three samples discussed above. Across the series we see that the hole cooling time scale varies greatly with surface coverage, decreasing by $\sim 2\times$ from CdSe-OA to CdSe-PTC. However, when treating the CdSe-PTC sample with $\text{Cd}(\text{Ac})_2$, we find that the hole cooling time scale recovers to match the CdSe-OA sample, while maintaining the red-shifted absorption spectrum induced by the PTC exchange (see Supporting Information, Figure S4). The reversibility of the increased hole cooling rate in CdSe-PTC upon treatment with $\text{Cd}(\text{Ac})_2$ suggests that at least *two* unique PTC species bind to the NC surface. Calculations have shown that PTC can bind to CdSe surfaces in monodentate, chelating, and bridging geometries^{32,44,45} and that each of these species has a different impact on a NC's radiative and nonradiative decay rates.⁴⁴ When CdSe-OA is treated with PTC, it is likely that a mixture of these different species form. Further treatment of these crystals with $\text{Cd}(\text{Ac})_2$ may preferentially remove one or more of these species. If the species removed is responsible for the change in hole cooling rate, that would explain the restoration that we observe of the hole cooling rate upon treatment of CdSe-PTC with $\text{Cd}(\text{Ac})_2$. This hypothesis is supported by prior work that has noted the photobrightening of CdSe-PTC solutions upon treatment with $\text{Cd}(\text{Ac})_2$.³¹ While this work ascribed photobrightening to the removal of unbound PTC molecules that diffusively encounter NCs and quench their emission by scavenging holes, our observation of changes in NC cooling dynamics on femtosecond time scales suggests that PL quenching by PTC is unlikely to be a diffusion-limited process but rather one involving molecules directly bound to the NC surface.

To explore the possibility that distinct PTC species may be attached to our NC surfaces, we have measured FT-IR spectra of drop-cast NC films. Figure 5A compares spectra of a CdSe-OA film before and after it has been soaked in a methanol

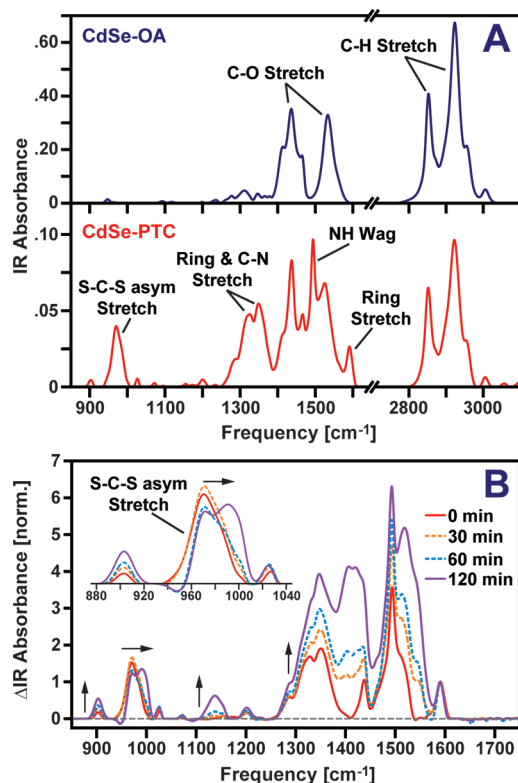


Figure 5. (A) FT-IR spectra of CdSe-OA films before (top, blue) and after PTC ligand exchange (bottom, red). Mode assignments are based on DFT calculations (see Supporting Information). (B) Difference FT-IR spectra of PTC exchanged CdSe-OA films as a function of time following Cd(Ac)₂ treatment. Plotted spectra have had contributions from oleate vibrational peaks removed by subtracting the CdSe-OA spectrum shown in (A) following normalization to the alkyl stretching transitions between 2800 and 3000 cm⁻¹. The resulting difference spectra are then normalized to the PTC ring stretching transition at 1590 cm⁻¹.

solution containing 10 mM PTC. Prior to PTC treatment, peaks due to the alkyl stretches of oleate ligands are observed just below 3000 cm⁻¹ and a pair of peaks are observed at 1432 and 1539 cm⁻¹ that are assigned to the symmetric and asymmetric carboxylate stretches of oleate bound to surface Cd atoms.⁴⁶ Upon PTC treatment, each of these peaks undergoes a noticeable decrease in amplitude, indicating that oleate is displaced from the NC surface. As these features disappear, three narrow peaks at 1590, 1494, and 970 cm⁻¹ are observed to grow in that are assigned to the C=C ring stretching, N-H wagging, and S-C-S asymmetric stretching modes of PTC on the basis of DFT calculations (see Supporting Information). In addition, a broad band centered at 1337 cm⁻¹ can be seen that arises from a combination of ring and C-N stretching modes. These results suggest that PTC indeed displaces oleate and binds to the surface of our CdSe NCs. While the magnitude of the decrease in the oleate stretching features should in principle allow us to estimate the amount of oleate displaced by PTC, extracting a quantitative value for the number of displaced ligands is complicated by the fact that our films experience some degree of NC material loss when treated with methanol. Hence, we refrain from making an estimate of this value at this point.

Figure 5B plots how the FT-IR spectra of CdSe-PTC films change upon exposure to Cd(Ac)₂. To highlight changes

associated with PTC ligand binding, peaks due to oleate have been removed from this data by subtracting the spectrum of CdSe-OA after scaling it to match the amplitude of the alkyl stretching peaks that appear from 2800 to 3000 cm⁻¹. With increased exposure time, we observe a decrease of all peaks in our spectra due to partial desorption of NCs from our film. To account for this effect, we have normalized our plotted spectra to the PTC C=C ring stretching peak at 1590 cm⁻¹ as this peak is predicted to display a minimal shift between different PTC binding geometries (see Supporting Information, Figure S5B).

Gains in amplitude upon Cd(Ac)₂ treatment can be seen near 1430 and 1540 cm⁻¹ and can be attributed to the symmetric and asymmetric stretching transitions of acetate molecules that coordinate to the surface. More interestingly, the normalized spectra reveal that the asymmetric S-C-S stretching peak at 970 cm⁻¹ decreases in amplitude and shifts to higher frequency with increasing exposure time to Cd(Ac)₂, suggesting that Cd(Ac)₂ alters the average geometry through which PTC molecules attach to CdSe. DFT calculations of PTC molecules bound to a CdSe {110} surface in chelating and two different bridging geometries indeed show that the asymmetric S-C-S stretch shifts between these different geometries (see Supporting Information, Figure S5). While the lack of quantitative agreement between our DFT calculations and experimental spectra prevents us from assigning the shifts we see in our measured FT-IR spectra to changes in the populations of specific surface bound species, our spectra and calculations suggest that different PTC species are present on our NC surfaces, one of which may be responsible for the rapid hole cooling that we observe in SR-TA measurements.

Discussion of Rapid Hole Cooling in CdSe-PTC. Excited holes often relax via EVET as they cannot access Auger channels due to the larger energy level spacing of the CB versus the VB. Though the exact details of this hole cooling mechanism are debated, recent reports have shown that EVET to both phonon modes^{47,48} and surface bound ligands^{26,49,50} contribute to hot carrier cooling. In particular, vibrations involving atoms directly anchored to the NC surface are expected to be important acceptors of excess energy due to their close proximity to the NC core. Examining the FT-IR spectrum shown in Figure 5A of CdSe-OA, we see that the symmetric and asymmetric carboxylate stretches fall at 1432 and 1539 cm⁻¹, respectively, placing both these modes close to the energy difference between the 2S_{3/2(h)} and 1S_{3/2(h)} states (~1685 cm⁻¹). Likewise, as these modes are associated with the oleate headgroup, they should be readily accessible to photoexcited holes. Taken together, these two effects suggest that EVET to these vibrational modes likely accounts for the observed rapid hole cooling in CdSe-OA.

Assuming that EVET similarly drives hole cooling upon PTC exchange, there are two explanations that may account for the increased hole cooling rate in CdSe-PTC: (1) hole cooling is facilitated by a single or collection of PTC modes that lie in close resonance with the 2S_{3/2(h)}-1S_{3/2(h)} energy gap when PTC is bound to CdSe in one particular geometry but not others, or (2) spatial extension of the hole increases the coupling strength of the carrier and ligand via direct wave function overlap. However, taking stock of the two-species model suggested by the recovery of the hole cooling kinetics of CdSe-PTC upon treatment with Cd(Ac)₂, both of these scenarios can be ruled out as we argue below.

On the basis of the energy gap between the X1 and X2 exciton states, whose value represents the energy spacing between the $2S_{3/2(h)}$ and $1S_{3/2(h)}$ states, we expect that a vibrational mode with a frequency of $\sim 1685\text{ cm}^{-1}$ would have the proper energetic alignment to accept excess energy from a hot hole. Examining the FT-IR spectrum of CdSe-PTC (Figure 5A), we see that modes assigned to stretching and bending of PTC's aromatic ring fall close to this energy difference and could possibly serve as accepting modes for the excess energy of a hot hole. To address scenario 1, we have used DFT to examine how the vibrational spectrum of PTC changes when it is bound in both chelating and bridging geometries to the $\{110\}$ surface of CdSe to determine if any of the modes described above experience large shifts tied to binding geometry (see Supporting Information, Figure S5C). While many of the ring modes do indeed display frequency shifts between these two geometries, many of these changes are small ($<20\text{ cm}^{-1}$) and are likely insufficient to rationalize a $2\times$ change in hole cooling rate due to the removal of PTC molecules that preferentially bind in one of these two different geometries.

The spectrum shown in Figure 5A also provides a hint as to why we can exclude scenario 2. While PTC does possess vibrational modes with frequencies close to 1600 cm^{-1} , these modes are primarily associated with stretching and bending motions of PTC's phenyl ring. However, prior work that has examined exciton delocalization imparted by PTC has shown that its S_2C-NH bridging group is responsible for most of the change in the density of states of CdSe's VB upon binding,³² indicating that hole density is preferentially associated with this group rather than PTC's phenyl ring. The spatial separation of the hole and phenyl ring would suggest that ring stretching and bending modes should be poor acceptors for the excess energy of hot holes. While vibrations involving the S_2C-NH binding group would be expected to couple strongly to hot holes and facilitate EVET, the spectra shown in Figure 5A indicate that these modes are significantly detuned from the $2S_{3/2(h)}-1S_{3/2(h)}$ energy gap. This suggests that EVET involving these modes must involve the simultaneous excitation of multiple lattice phonons, reducing the likelihood of this event. On the basis of these arguments, we believe that we can rule out EVET to PTC as the primary pathway leading to hole cooling.

As vibrational relaxation appears to be insufficient to explain our results, we have developed an alternative scenario to explain this rapid hole cooling phenomenon. SR-TA tracks hole cooling by measuring a loss of amplitude of the A1-induced absorption band. However, if excited holes were to be physically removed from a NC, this would similarly lead to a loss of A1-induced absorption. Thus, a scenario that can explain our results is one wherein PTC molecules bound to the NC core in a particular geometry trap hot holes, extracting them from the NC. This picture is consistent with prior work that demonstrated that PTC can quench the photoluminescence (PL) of CdSe NCs.³¹ However, while this work assumed that PTC quenching was diffusive in nature, involving unbound PTC molecules in solution, the femtosecond rate of quenching suggested by our results indicates that it must involve a species directly bound to the NC surface. Hence, we hypothesize that rather than unbound PTC scavenging holes as previously reported, a subset of PTC molecules bound to the surface can rapidly remove photoexcited holes from the NC core, quenching photoluminescence (PL) and increasing the apparent rate of carrier cooling.

This mechanism for fast hole trapping in CdSe-PTC is supported by steady-state PL measurements, shown in Figure 6.

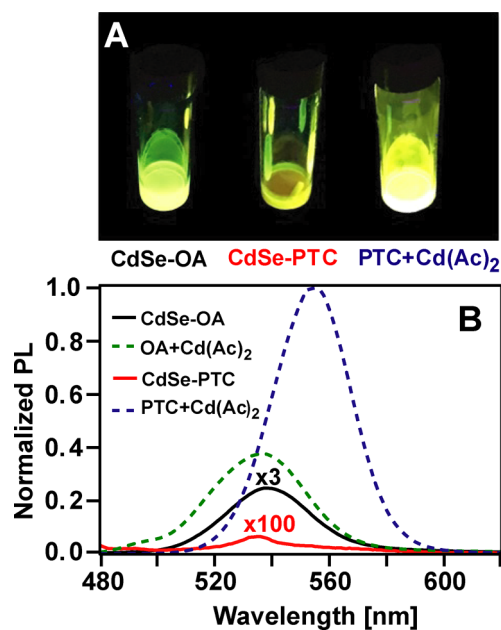


Figure 6. (A) Photograph depicting photoluminescence of CdSe-OA, CdSe-PTC, and PTC + Cd(Ac)₂ under 365 nm excitation. (B) PL spectra of CdSe-OA (black), OA + Cd(Ac)₂ (green dashed), CdSe-PTC (red), and PTC + Cd(Ac)₂ (blue dashed). Spectra are plotted relative to the PTC + Cd(Ac)₂ emission maximum.

Figure 6B shows the relative emission spectrum of CdSe-OA, CdSe-PTC, PTC + Cd(Ac)₂, and a control sample composed of CdSe-OA with added Cd(Ac)₂ (denoted OA + Cd(Ac)₂). From the relative QY from each sample we see that PTC-capped NCs are highly quenched, displaying a QY that is only 0.79% of that of CdSe-OA. However, this effect is clearly reversed upon addition of Cd(Ac)₂. In the PTC + Cd(Ac)₂ sample we see recovery of the photoluminescence QY exceeding the CdSe-OA sample as well as the control sample OA + Cd(Ac)₂. This increased photoluminescence intensity of PTC + Cd(Ac)₂ shows that only a small portion of the gain in photoluminescence intensity can be attributed to passivating surface electron traps. Therefore, it is likely that some oscillator strength is borrowed from the PTC ligand, as predicted by previous work,^{31,32} which would account for the remaining increase in photoluminescence QY.

In addition to the PL data, transient absorption and time-correlated single photon counting (TCSPC) kinetics provide evidence for a hole-trapping mechanism induced by PTC exchange. Examining the PA absorption feature that reports on the presence of trapped holes,^{34,41,42} we find that for each of the CdSe samples described above this feature develops with an ~ 180 fs time constant (see Supporting Information, Figure S6), indicating that all of our CdSe suspensions rapidly trap holes. To determine the percentage of holes that populate trap sites, we can compare the amplitude of the PA band to the initial amplitude of the B1 bleach as this reports on the number of excited electrons placed in the $1S_{(e)}$ state by our excitation pulse (Table 1). Interestingly, we find that the PA:B1 ratio decreases by nearly $2\times$ for CdSe-PTC relative to CdSe-OA. This suggests that CdSe-PTC traps fewer holes at sites that contribute to the PA absorption feature. While this result may

Table 1. Maximum Amplitude of the PA (Averaged from 600 to 750 nm) and B1 Spectral Features^a

sample	PA peak amplitude [mOD]	B1 peak amplitude [mOD]	PA:B1 ratio (%)
CdSe-OA	0.185	18.8	0.98
CdSe-PTC	0.11	19.4	0.57
PTC + Cd(Ac) ₂	0.18	13.5	1.33

^aThe ratio of these amplitudes reflects the relative number of photoexcited holes trapped in each sample. Absolute values of the B1 amplitude have been used in calculating the PA:B1 ratio due to the opposite sign of these features.

at first seem counterintuitive if PTC treatment induces additional hole traps, it is consistent with a picture wherein PTC-induced traps are strongly ligand-associated rather than residing on the NC surface or core. The PA absorption feature arises from lattice defects and unpassivated surface sites that generate midgap states. As these species reside on the NC itself, they can optically access states within the NC VB, leading to the appearance of the PA absorption band. In contrast, if PTC creates hole traps that primarily reside on the ligand, absorption transitions between these PTC-centered states and deeper states within the NC valence band are expected to have low oscillator strength due to their spatial separation. Thus, trapping a hole on a PTC molecule would lead to a decrease of the PA feature rather than an increase. Treatment of CdSe-PTC with Cd(Ac)₂ increases the PA:B1 ratio, suggesting that it removes PTC-associated hole traps.

The long-time kinetics of the B1 feature also support a scenario wherein PTC creates additional ligand-associated hole traps. Figure 7A shows the recovery of the B1 feature up to 1.65

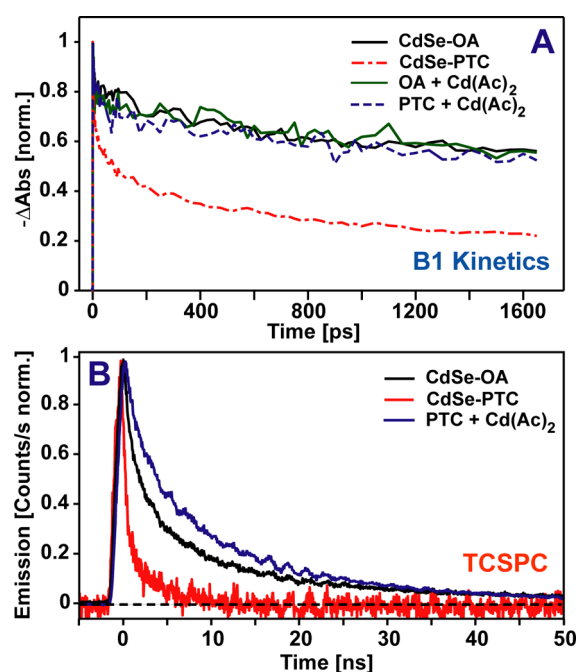


Figure 7. (A) Normalized decay traces of the B1 spectral feature for X1 pumped CdSe-OA (black), CdSe-PTC (red dash dot), PTC + Cd(Ac)₂ (blue dashed), and OA + Cd(Ac)₂ (green). (B) TCSPC decays for CdSe-OA (black), CdSe-PTC (red), and PTC + Cd(Ac)₂ (blue). CdSe-PTC shows an instrument limited decay, indicating relaxation occurs primarily through nonradiative pathways.

ns after photoexcitation for each of the three NC samples. The CdSe-PTC sample shows a rapid, nonexponential decay of the B1 amplitude within the first 100 ps followed by an additional slow decay that can be fit well by an exponential with a 2.7 ns time constant. This rapid decay is echoed by TCSPC measurements (Figure 7B) that are dominated by an instrument-limited decay followed by a slower decay over 2.7 ns. This behavior is in stark contrast to that of CdSe-OA, which after a short ~ 30 ps decay exhibits a 5.2 ns exponential decay that is consistent with TCSPC measurements. As the B1 amplitude tracks the population of electrons in the $1S_{(e)}$ state, these results indicate that PTC treatment creates a new pathway that either traps electrons or leads to their recombination with holes. While we do not have definitive evidence that can differentiate electron trapping from electron–hole recombination, one piece of data that suggests that PTC-trapped holes nonradiatively recombine with $1S_{(e)}$ electrons comes from the PA band, which shows a decay that matches the recovery of the CdSe-PTC B1 bleach (see Supporting Information, Figure S8). This is consistent with a scenario wherein nonradiative recombination between PTC-associated trapped holes and $1S_{(e)}$ electrons occurs rapidly, leading to the sub-100 ps B1 bleach decay. Transfer of trapped holes from NC defects to PTC-associated traps over longer time scales would then lead to a decay of the PA and B1 features that closely track one another due to rapid recombination of $1S_{(e)}$ electrons with PTC-associated traps. As with the PA:B1 ratio described in Table 1, upon addition of Cd(Ac)₂ to CdSe-PTC, we see that both the rapid decay of the B1 amplitude and TCSPC decay recover, indicating the elimination of PTC-associated traps.

To summarize, our work suggests that there are likely two different PTC species attached to CdSe NC surfaces following ligand exchange. Further treatment of CdSe-PTC with Cd(Ac)₂ results in a drastic change in both intraband hole cooling and global relaxation rates, measured by transient absorption experiments, as well as increased photoluminescence QY and lifetime. These findings led us to conclude that Cd(Ac)₂ removes a species that facilitates the population of nonemissive, hole trap states on a sub-picosecond time scale after photoexcitation. The removal of this species eliminates access to this trapping pathway, allowing photoexcited holes to cool via EVET, similar to CdSe-OA.

Although definitive assignment of the hole trapping species is not possible with the given data, PTC bound in a monodentate geometry is likely to serve as a hole trap as it has an exposed lone pair. The existence of such species is supported by simulations by Azpiroz and De Angelis that showed their presence on CdSe NCs, albeit in small numbers.³² Moreover, a scenario wherein monodentate PTC molecules act as hole traps is also consistent with our observation that Cd(Ac)₂ treatment results in a removal of these traps. The addition of Cd²⁺ atoms repairs surface defects, as indicated by an increase in PL quantum efficiency and a slight red-shift in the absorption maximum of CdSe-OA samples. The addition of Cd²⁺ atoms to a NC surface would provide additional attachment sites for PTC molecules, likely reducing the number coordinated to the surface in a monodentate geometry. Figure 8 depicts our proposal for how PTC treatment and subsequent Cd(Ac)₂ treatment modify the surface of CdSe NCs. EVET to oleate ligands dominates hole cooling in CdSe-OA NCs. Following PTC exchange fast transfer of photoexcited holes to monodentate PTC molecules can occur. Hole relaxation is

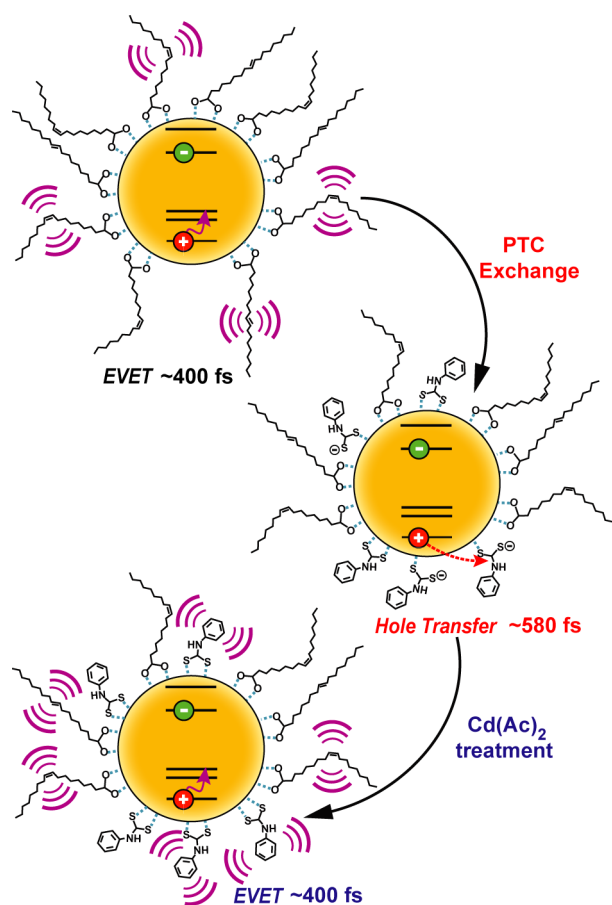


Figure 8. Cartoon depiction of ligand-dependent hole cooling mechanisms. PTC exchange induces fast hole transfer (~ 580 fs) to PTC in CdSe-PTC with monodentate PTC as the hole acceptor. Removal of monodentate PTCs by $\text{Cd}(\text{Ac})_2$ leads to hole cooling via an EVET pathway, similar to CdSe-OA.

again dominated by EVET following removal of monodentate PTC molecules by $\text{Cd}(\text{Ac})_2$.

As the observed hole relaxation rate in CdSe-PTC represents a sum of the rates for both the formation of PTC-associated traps and hole cooling, we can extract a rate for PTC-associated trap formation assuming the intrinsic time scale for hole cooling is unchanged by PTC treatment. Under this assumption, we find that the time scale for PTC-associated trap population is 580 fs ($1/236 \text{ fs} = 1/580 \text{ fs} + 1/398 \text{ fs}$). As our measurements cannot determine the number of PTC-associated traps per NC, this time scale represents an upper bound on the rate of trapping at these sites as it is the product of the rate of populating a single PTC-associated trap and the number of trap sites on a NC.

IV. CONCLUSIONS AND OUTLOOK

We have presented evidence that the EDL PTC binds to CdSe NC surfaces in multiple geometries and that these geometries greatly impact the NC's excited state dynamics. Specifically, we have isolated the effects of two different species by using $\text{Cd}(\text{Ac})_2$ to alter the average binding geometry of PTC molecules bound to the surface of CdSe NCs. By measuring the hole cooling rate for different NC samples, we have shown that a subset of PTC molecules bound to the surface can trap photoexcited holes and facilitate nonradiative recombination. In contrast, NCs that have been treated with $\text{Cd}(\text{Ac})_2$ relax

primarily through radiative recombination, suggesting removal of these quenching PTC molecules.

On the basis of SR-TA measurements, we find that in CdSe-PTC holes populate trap states in ~ 580 fs, indicating that fast hole transfer to the PTC ligand can compete with carrier cooling to the band edge. Upon treatment of CdSe-PTC with $\text{Cd}(\text{Ac})_2$ we see the hole cooling rate recover to similar values measured for CdSe-OA (~ 400 fs), and the photoluminescence QY greatly increases beyond that of the NL-capped NCs. This data indicates that $\text{Cd}(\text{Ac})_2$ removes a surface-bound species that introduces ligand associated trap states, while maintaining the absorption red-shift induced from the addition of PTC to the NC solution.

This last result is interesting in that it shows that EDLs do not necessarily drive rapid carrier cooling via EVET despite extended wave function overlap between the NC core and these ligands. Rather, we see that hot carrier cooling dynamics appear to be highly dependent on both the binding geometry of the EDL and the details of its vibrational density of states. Indeed, we find that OA is likely a major contributor to hot hole relaxation in the NCs we have examined due to good energetic matching of the vibrational frequencies associated with its carboxylate binding group and the splitting between the NC $2\text{S}_{3/2(\text{h})}$ and $1\text{S}_{3/2(\text{h})}$ states. Exchange of OA for a different capping NL coupled with careful control of the PTC binding geometry could perhaps further extend the lifetime of hot holes and allow their extraction. This work informs the use of EDLs to design systems that facilitate hot hole transfer and improved carrier transport in thin films.

■ ASSOCIATED CONTENT

Supporting Information

The Supporting Information is available free of charge on the ACS Publications website at DOI: 10.1021/acs.jpcc.6b08178.

Absorption spectra documenting PTC exchange kinetics over 60 h; a discussion of IRF determination and time-zero correction for transient absorption spectra; control SR-TA measurements performed on OA + $\text{Cd}(\text{Ac})_2$ samples; description of DFT calculations for PTC molecules bound to CdSe {110}; kinetic fits to transient absorption and TCSPC data (PDF)

■ AUTHOR INFORMATION

Corresponding Author

*E-mail: roberts@cm.utexas.edu, Tel (512) 475-9450 (S.T.R.).

ORCID

Graeme Henkelman: 0000-0002-0336-7153

Sean T. Roberts: 0000-0002-3322-3687

Notes

The authors declare no competing financial interest.

■ ACKNOWLEDGMENTS

This work was supported by the Air Force Office of Scientific Research (S.T.R. Grant FA9550-15-1-0344), the Robert A. Welch Foundation (S.T.R. Grant F-1885; G.H. Grant F-1481), the National Science Foundation (S.T.R. Grant CHE-1610412), and start-up funding provided by the University of Texas at Austin (S.T.R.). M.S.A. acknowledges additional support from the Bennie Walker Foundation. M.C.B. acknowledges support from an Undergraduate Research Fellowship, and S.T.R. acknowledges a Research Grant, both provided by

the Office of the Vice President for Research at the University of Texas at Austin. This work was performed in part at the Center for Nano- and Molecular Science (CNM), a member of the National Nanotechnology Coordinated Infrastructure (NNCI), which is supported by the National Science Foundation (Grant ECCS-1542202). DFT calculations were carried out at the Texas Advanced Computing Center (TACC). M.S.A. and S.T.R. also acknowledge Dr. Emily Weiss for helpful correspondence regarding PTC surface functionalization and Dr. Gordana Dukovic for helpful discussions concerning the interpretation of state-resolved transient absorption data.

REFERENCES

- (1) Ginger, D. S.; Greenham, N. C. Charge Injection and Transport in Films of CdSe Nanocrystals. *J. Appl. Phys.* **2000**, *87*, 1361–1368.
- (2) Li, G.-S.; Zhang, D.-Q.; Yu, J. C. A New Visible-Light Photocatalyst: CdS Quantum Dots Embedded Mesoporous TiO₂. *Environ. Sci. Technol.* **2009**, *43*, 7079–7085.
- (3) Chang, C. M.; Orchard, K. L.; Martindale, B. C. M.; Reiser, E. Ligand Removal from CdS Quantum Dots for Enhanced Photocatalytic H₂ Generation in pH Neutral Water. *J. Mater. Chem. A* **2016**, *4*, 2856–2862.
- (4) Wang, C.; Thompson, R. L.; Ohodnicki, P.; Baltrus, J.; Matranga, C. Size-Dependent Photocatalytic Reduction of CO₂ with PbS Quantum Dot Sensitized TiO₂ Heterostructured Photocatalysts. *J. Mater. Chem.* **2011**, *21*, 13452–13457.
- (5) Carey, G. H.; Abdelhady, A. L.; Ning, Z.; Thon, S. M.; Bakr, O. M.; Sargent, E. H. Colloidal Quantum Dot Solar Cells. *Chem. Rev.* **2015**, *115*, 12732–12763.
- (6) Koleilat, G. I.; Levina, L.; Shukla, H.; Myrskog, S. H.; Hinds, S.; Pattanyus-Abraham, A. G.; Sargent, E. H. Efficient, Stable Infrared Photovoltaics Based on Solution-Cast Colloidal Quantum Dots. *ACS Nano* **2008**, *2*, 833–840.
- (7) Kim, G.-H.; Garcia de Arquer, F. P.; Yoon, Y. J.; Lan, X.; Liu, M.; Voznyy, O.; Yang, Z.; Fan, F.; Ip, A. H.; Kanjanaboos, P.; Hoogland, S.; Kim, J. Y.; Sargent, E. H. High-Efficiency Colloidal Quantum Dot Photovoltaics via Robust Self-Assembled Monolayers. *Nano Lett.* **2015**, *15*, 7691–7696.
- (8) Ning, Z.; Ren, Y.; Hoogland, S.; Voznyy, O.; Levina, L.; Stadler, P.; Lan, X.; Zhitomirsky, D.; Sargent, E. H. All-Inorganic Colloidal Quantum Dot Photovoltaics Employing Solution-Phase Halide Passivation. *Adv. Mater.* **2012**, *24*, 6295–6299.
- (9) Zarghami, M. H.; Liu, Y.; Gibbs, M.; Gebremichael, E.; Webster, C.; Law, M. p-Type PbSe and PbS Quantum Dot Solids Prepared with Short-Chain Acids and Diacids. *ACS Nano* **2010**, *4*, 2475–2485.
- (10) Jang, J.; Dolzhenkov, D. S.; Liu, W.; Nam, S.; Shim, M.; Talapin, D. V. Solution-Processed Transistors using Colloidal Nanocrystals with Composition-Matched Molecular “Solders”: Approaching Single Crystal Mobility. *Nano Lett.* **2015**, *15*, 6309–6317.
- (11) Zotti, G.; Vercelli, B.; Berlin, A.; Virgili, T. Multilayers of CdSe Nanocrystals and Bis(dithiocarbamate) Linkers Displaying Record Photoconduction. *J. Phys. Chem. C* **2012**, *116*, 25689–25693.
- (12) Lu, H.; Joy, J.; Gaspar, R. L.; Bradforth, S. E.; Brutchey, R. L. Iodide-Passivated Colloidal PbS Nanocrystals Leading to Highly Efficient Polymer:Nanocrystal Hybrid Solar Cells. *Chem. Mater.* **2016**, *28*, 1897–1906.
- (13) Frederick, M. T.; Weiss, E. A. Relaxation of Exciton Confinement in CdSe Quantum Dots by Modification with a Conjugated Dithiocarbamate Ligand. *ACS Nano* **2010**, *4*, 3195–3200.
- (14) Wagner, S.; Gleskova, H.; Cheng, I.-C.; Wu, M. Silicon for Thin-Film Transistors. *Thin Solid Films* **2003**, *430*, 15–19.
- (15) Kuo, Y. Thin Film Transistor Technology - Past, Present, and Future. *Electrochem. Soc. Interface* **2013**, *22*, 55–61.
- (16) Wu, K.; Du, Y.; Tang, H.; Chen, Z.; Lian, T. Efficient Extraction of Trapped Holes from Colloidal CdS Nanorods. *J. Am. Chem. Soc.* **2015**, *137*, 10224–10230.
- (17) Utterback, J. K.; Wilker, M. B.; Brown, K. A.; King, P. W.; Eaves, J. D.; Dukovic, G. Competition between Electron Transfer, Trapping, and Recombination in CdS Nanorod–Hydrogenase Complexes. *Phys. Chem. Chem. Phys.* **2015**, *17*, 5538–5542.
- (18) Schnitzenbaumer, K. J.; Labrador, T.; Dukovic, G. Impact of Chalcogenide Ligands on Excited State Dynamics in CdSe Quantum Dots. *J. Phys. Chem. C* **2015**, *119*, 13314–13324.
- (19) Lian, S.; Weinberg, D. J.; Harris, R. D.; Kodaimati, M. S.; Weiss, E. A. Subpicosecond Photoinduced Hole Transfer from a CdS Quantum Dot to a Molecular Acceptor Bound Through an Exciton-Delocalizing Ligand. *ACS Nano* **2016**, *10*, 6372–6382.
- (20) Yu, S.; Kim, Y. H.; Lee, S. Y.; Song, H. D.; Yi, J. Hot-Electron-Transfer Enhancement for the Efficient Energy Conversion of Visible Light. *Angew. Chem., Int. Ed.* **2014**, *53*, 11203–11207.
- (21) Dong, Y.; Rossi, D.; Parobek, D.; Son, D. H. Nonplasmonic Hot-Electron Photocurrents from Mn-Doped Quantum Dots in Photoelectrochemical Cells. *ChemPhysChem* **2016**, *17*, 660–664.
- (22) Klimov, V. I.; McBranch, D. W. Femtosecond 1P-to-1S Electron Relaxation in Strongly Confined Semiconductor Nanocrystals. *Phys. Rev. Lett.* **1998**, *80*, 4028–4031.
- (23) Brus, L. E. Electron–electron and Electron-hole Interactions in Small Semiconductor Crystallites: The Size Dependence of the Lowest Excited Electronic State. *J. Chem. Phys.* **1984**, *80*, 4403–4409.
- (24) Norris, D. J.; Bawendi, M. G. Measurement and Assignment of the Size-dependent Optical Spectrum in CdSe Quantum Dots. *Phys. Rev. B: Condens. Matter Mater. Phys.* **1996**, *53*, 16338–16346.
- (25) Peterson, M. D.; Cass, L. C.; Harris, R. D.; Edme, K.; Sung, K.; Weiss, E. A. The Role of Ligands in Determining the Exciton Relaxation Dynamics in Semiconductor Quantum Dots. *Annu. Rev. Phys. Chem.* **2014**, *65*, 317–339.
- (26) Lifshitz, E. Evidence in Support of Exciton to Ligand Vibrational Coupling in Colloidal Quantum Dots. *J. Phys. Chem. Lett.* **2015**, *6*, 4336–4347.
- (27) Guyot-Sionnest, P.; Shim, M.; Matranga, C.; Hines, M. Intraband Relaxation in CdSe Quantum Dots. *Phys. Rev. B: Condens. Matter Mater. Phys.* **1999**, *60*, R2181–R2184.
- (28) Sewall, S. L.; Cooney, R. R.; Anderson, K. E. H.; Dias, E. A.; Kambhampati, P. State-to-state Exciton Dynamics in Semiconductor Quantum Dots. *Phys. Rev. B: Condens. Matter Mater. Phys.* **2006**, *74*, 235328.
- (29) Frederick, M. T.; Amin, V. A.; Cass, L. C.; Weiss, E. A. A Molecule to Detect and Perturb the Confinement of Charge Carriers in Quantum Dots. *Nano Lett.* **2011**, *11*, 5455–5460.
- (30) Frederick, M. T.; Amin, V. A.; Weiss, E. A. Optical Properties of Strongly Coupled Quantum Dot–Ligand Systems. *J. Phys. Chem. Lett.* **2013**, *4*, 634–640.
- (31) Jin, S.; Harris, R. D.; Lau, B.; Aruda, K. O.; Amin, V. A.; Weiss, E. A. Enhanced Rate of Radiative Decay in CdSe Quantum Dots upon Adsorption of an Exciton-Delocalizing Ligand. *Nano Lett.* **2014**, *14*, 5323–5328.
- (32) Azpiroz, J. M.; De Angelis, F. Ligand Induced Spectral Changes in CdSe Quantum Dots. *ACS Appl. Mater. Interfaces* **2015**, *7*, 19736–19745.
- (33) Kambhampati, P. State-resolved Exciton Dynamics in Quantum Dots. *Proc. SPIE* **2010**, *7758*, 77580R.
- (34) Sewall, S. L.; Cooney, R. R.; Anderson, K. E. H.; Dias, E. A.; Sagar, D. M.; Kambhampati, P. State-resolved Studies of Biexcitons and Surface Trapping Dynamics in Semiconductor Quantum Dots. *J. Chem. Phys.* **2008**, *129*, 084701.
- (35) Carion, O.; Mahler, B.; Pons, T.; Dubertret, B. Synthesis, Encapsulation, Purification and Coupling of Single Quantum Dots in Phospholipid Micelles for Their Use in Cellular and in Vivo Imaging. *Nat. Protoc.* **2007**, *2*, 2383–2390.
- (36) Frederick, M. T.; Amin, V. A.; Swenson, N. K.; Ho, A. Y.; Weiss, E. A. Control of Exciton Confinement in Quantum Dot–Organic Complexes through Energetic Alignment of Interfacial Orbitals. *Nano Lett.* **2013**, *13*, 287–292.
- (37) Yu, W. W.; Qu, L.; Guo, W.; Peng, X. Experimental Determination of the Extinction Coefficient of CdTe, CdSe, and CdS Nanocrystals. *Chem. Mater.* **2003**, *15*, 2854–2860.

- (38) Norris, D. J. Electronic Structure in Semiconductor Nanocrystals. In *Semiconductor and Metal Nanocrystals: Synthesis and Electronic and Optical Properties*; Klimov, V. I., Ed.; CRC Press: New York, 2003.
- (39) Klimov, V. I. Spectral and Dynamical Properties of Multiexcitons in Semiconductor Nanocrystals. *Annu. Rev. Phys. Chem.* **2007**, *58*, 635–673.
- (40) Klimov, V.; Hunsche, S.; Kurz, H. Biexciton Effects in Femtosecond Nonlinear Transmission of Semiconductor Quantum Dots. *Phys. Rev. B: Condens. Matter Mater. Phys.* **1994**, *50*, 8110–8113.
- (41) McArthur, E. A.; Morris-Cohen, A. J.; Knowles, K. E.; Weiss, E. A. Charge Carrier Resolved Relaxation of the First Excitonic State in CdSe Quantum Dots Probed with Near-Infrared Transient Absorption Spectroscopy. *J. Phys. Chem. B* **2010**, *114*, 14514–14520.
- (42) Huang, J.; Huang, Z.; Jin, S.; Lian, T. Exciton Dissociation in CdSe Quantum Dots by Hole Transfer to Phenothiazine. *J. Phys. Chem. C* **2008**, *112*, 19734–19738.
- (43) Klimov, V. I. Optical Nonlinearities and Ultrafast Carrier Dynamics in Semiconductor Nanocrystals. *J. Phys. Chem. B* **2000**, *104*, 6112–6123.
- (44) Swenson, N. K.; Ratner, M. A.; Weiss, E. A. Computational Study of the Influence of the Binding Geometries of Organic Ligands on the Photoluminescence Quantum Yield of CdSe Clusters. *J. Phys. Chem. C* **2016**, *120*, 6859–6868.
- (45) Swenson, N. K.; Ratner, M. A.; Weiss, E. A. Computational Study of the Resonance Enhancement of Raman Signals of Ligands Adsorbed to CdSe Clusters through Photoexcitation of the Cluster. *J. Phys. Chem. C* **2016**, *120*, 20954.
- (46) Chen, O.; Yang, Y.; Wang, T.; Wu, H.; Niu, C.; Yang, J.; Cao, Y. C. Surface-Functionalization-Dependent Optical Properties of II–VI Semiconductor Nanocrystals. *J. Am. Chem. Soc.* **2011**, *133* (43), 17504–17512.
- (47) Fernee, M. J.; Littleton, B. N.; Cooper, S.; Rubinsztein-Dunlop, H.; Gomez, D. E.; Mulvaney, P. Acoustic Phonon Contributions to the Emission Spectrum of Single CdSe Nanocrystals. *J. Phys. Chem. C* **2008**, *112*, 1878–1884.
- (48) Sagar, D. M.; Cooney, R. R.; Sewall, S. L.; Dias, E. A.; Barsan, M. M.; Butler, I. S.; Kambhampati, P. Size Dependent, State-Resolved Studies of Exciton-Phonon Couplings in Strongly Confined Semiconductor Quantum Dots. *Phys. Rev. B: Condens. Matter Mater. Phys.* **2008**, *77*, 235321.
- (49) Cooney, R. R.; Sewall, S. L.; Dias, E. A.; Sagar, D. M.; Anderson, K. E. H.; Kambhampati, P. Unified Picture of Electron and Hole Relaxation Pathways in Semiconductor Quantum Dots. *Phys. Rev. B: Condens. Matter Mater. Phys.* **2007**, *75*, 245311.
- (50) Kilina, S.; Velizhanin, K. A.; Ivanov, S.; Prezhdo, O. V.; Tretiak, S. Surface Ligands Increase Photoexcitation Relaxation Rates in CdSe Quantum Dots. *ACS Nano* **2012**, *6*, 6515–6524.